frontiers | Frontiers in Energy Research

TYPE Original Research
PUBLISHED 16 September 2022
DOI 10.3389/fenrg.2022.998921

OPEN ACCESS

EDITED BY
Lin Qiu,
University of Science and Technology Beijing, China

REVIEWED BY
Hossam A. Gabbar,
Ontario Tech University, Canada
Gevork B. Gharehpetian,
Amirkabir University of Technology, Iran

*CORRESPONDENCE
He Cai,
caihe@scut.edu.cn

SPECIALTY SECTION
This article was submitted to Energy Storage,
a section of the journal Frontiers in Energy Research

RECEIVED 20 July 2022
ACCEPTED 17 August 2022
PUBLISHED 16 September 2022

CITATION
Cai H (2022), Asymptotic internal model based coordination of a flywheel energy storage matrix system.
Front. Energy Res. 10:998921.
doi: 10.3389/fenrg.2022.998921

Asymptotic internal model based coordination of a flywheel energy storage matrix system

He Cai *

School of Automation Science and Engineering, South China University of Technology, Guangzhou, China

This paper considers a dual objective distributed coordination problem for a flywheel energy storage matrix system. On one hand, the power output of the entire flywheel energy storage matrix system should track its reference command, which is generated by a linear command generator. On the other hand, the state-of-energy of all the flywheels should be balanced. In contrast to the existing result which employed a common state-of-energy generator as the external model by making use of global system information. By taking advantage of average consensus algorithms, a novel asymptotic internal model based control method is proposed in this paper which eliminates the need of the external model. It is proven that the steady-state of the asymptotic internal model turns out to be a common state-of-energy generator for all the flywheels under the composite average consensus algorithms, which lends itself to the solution to the dual objective distributed coordination problem. Comprehensive case studies in different scenarios are conducted to examine the performance of the proposed control method.

KEYWORDS

flywheel energy storage system, average consensus, internal model, multiagent system, state of energy

1 Introduction

Flywheels have many merits in comparison with other types of energy storage units, such as high energy density, fast response, low maintenance, long life-time and environmental friendliness. For example, the traditional applications of flywheel energy storage include power quality improvement Akram et al. (2020); Jia et al. (2022) and uninterruptible power supply Gengji and Ping (2016); Li et al. (2018). While, for these scenarios, in contrast to flywheels, batteries or super-capacitors can barely last for over a decade since the cycles for these applications are too frequent. By storing energy as the kinetic energy in the rotational mass,

Abbreviations: AIM, asymptotic internal model; CG, command generator; DCO, distributed command observer; FESMS , flywheel energy storage matrix system; SOC, state-of-charge; SOE, state-of-energy.

flywheel energy storage systems can be implemented in many practical situations Amiryar and Pullen (2017); Arani et al. (2017); Mousavi et al. (2017); Faisal et al. (2018); Olabi et al. (2021); Choudhury (2021); Li and Palazzolo (2022). There have been thus far various design and control methods developed for flywheel energy storage systems, such as the neutral-point potential control Li Z. et al. (2022), active disturbance rejection Chang et al. (2015); Ghanaatian and Lotfifard (2019), wide speed range operation Zhang and Yang (2017), DC-link voltage control Zhang and Yang (2018); Gong et al. (2020), robust control Zhang et al. (2021); Liang et al. (2022), and learning based intelligent control He et al. (2022); Yin and Li (2022), just to name a few. On the other hand, flywheels have recently found applications in many new areas, such as energy management for railways Canova et al. (2022); Li J. et al. (2022), offshore wind farm power transmission Daoud et al. (2016); Tomczewski et al. (2019), vehicle energy harvesting Ahamad et al. (2019); Thormann et al. (2021), and so on.

Though flywheels are competitive in energy density, they have relatively low power density. To solve this issue, a possible way is to connect multiple flywheels together into a flywheel energy storage matrix system (FESMS). An important application scenario for FESMS is to support wind turbine generator system Cao et al. (2016); Lai et al. (2018); Wei et al. (2018); Sun et al. (2020). Some pioneering works have been established on the design and control of FESMS. In Cao et al. (2016), a fully distributed dispatching algorithm for FESMS was proposed, which does not rely on central controller and requires no prior knowledge of the communication network topology. Lai et al. (2018) developed a coordination control scheme consisting of a charge–discharge control strategy and a safeguard mechanism for a FESMS with an aggregated connection topology. A simple but effective neuroadaptive PID control algorithm for adjusting the flywheel speed to achieve timely charge or discharge of the unit was derived. To solve the problems of over-charging, over-discharging, and overcurrent caused by traditional charging–discharging control strategies, Shi et al. (2019) proposed a charging–discharging coordination control strategy based on the equal incremental principle, which aims to minimize the total loss and establish a mathematical model of optimal coordination control with the constraints of total charging–discharging power, rated power limit, over-charging, over-discharging, and overcurrent. Two novel control strategies based on event triggering and self-triggering were studied in Sun et al. (2020) for the cooperative operation of a FESMS. Different from the traditional sampling mechanism, a periodic sampling-based event-triggered condition based on the disagreement vector and the measurement error was proposed for solving the FESMS dispatch problem.

Regarding the upper level coordination of a large scale integrated energy storage system, there are mainly two fundamental control objectives. On one hand, the total power output of the integrated energy storage system should meet its reference command so as to provide timely qualified service to the grid, such as frequency or voltage regulation. On the other hand, the state-of-charge (SOC) or state-of-energy (SOE) of all the energy storage units should be balanced so that the maximum power capacity of the integrated energy storage system can be maintained for all the time. Seminal works on the dual objective coordination of battery energy storage systems can be found in Lu et al. (2014, 2015); Cai and Hu (2016); Morstyn et al. (2016, 2018). While, there have been less efforts devoted to the dual objective coordination of FESMS. In Zhang et al. (2022), allocation of the total charging and discharging power of wind farms to individual flywheel unit was considered, where SOE consensus algorithms under both undirected and unbalanced directed graphs were developed. Nevertheless, Zhang et al. (2022) does not consider the specific dynamics of the flywheel systems. In contrast, Liu et al. (2021) studied the dual objective coordination of FESMS taking into consideration the detailed flywheel dynamics, where it is revealed that the dual control objective can be achieved if and only if the SOE of each flywheel converges to a common SOE generator, which was shown to be a nonautonomous dynamic system with the reference command for the entire FESMS as the external input. By explicitly implementing this nonautonomous dynamic system as an external model, the coordination problem for the FESMS was solved in Liu et al. (2021) by a distributed control approach. However, a drawback of this control approach lies in that the implementation of the external model depends on the system parameters of all the flywheel systems, which are global system information. Therefore, this control approach might not be realistic in some practical cases.

To further solve this issue, in this paper, a novel control method is proposed to solve the dual objective coordination problem for a FESMS. By taking advantage of average consensus algorithms, a novel asymptotic internal model based control method is proposed in this paper which eliminates the need of the external model as in Liu et al. (2021). It is proven that the steady-state of the asymptotic internal model turns out to be a common state-of-energy generator for all the flywheels under the composite average consensus algorithms. Then, by driving the SOE of the flywheel to this asymptotic internal model, the dual objective coordination problem for FESMS can be solved in a fully distributed way. Moreover, it is shown by numerical simulations that the proposed control method shows potential robustness against unreliable communication links, power output saturation, and inter-system time-delay issues.

The rest of this paper is organized as follows. The notation used in this paper are summarized in **Section 3**. **Section 4** introduces the problem formulation. The design and analysis of the asymptotic internal model based coordination are detailed

in Section 5. Comprehensive case studies are given in Section 6. Finally, this paper is concluded by Section 7.

2 Notation

$\mathbb{R}$ denotes the real number field. For $x_i \in \mathbb{R}^{n_i}$, $i = 1,\ldots,m$, $\mathrm{col}(x_1,\ldots,x_m) = [x_1^T,\ldots,x_m^T]^T$. $1_n = \mathrm{col}(1,\ldots,1) \in \mathbb{R}^n$. A graph $\mathcal{G} = (\mathcal{V},\mathcal{E})$ consists of a node set $\mathcal{V} = \{1,\ldots,N\}$ and an edge set $\mathcal{E} \subseteq \mathcal{V}\times\mathcal{V}$. For $i,j = 1,2,\ldots,N$, $i \neq j$, an edge of $\mathcal{E}$ from node i to node j is denoted by (i,j), and node i is called a neighbor of node j. Let $\mathcal{N}_i$ denote the set consisting of all the neighbors of node i. If $(i,j) \in \mathcal{E}$ if and only if $(j,i) \in \mathcal{E}$, then the edge (i,j) is called undirected. If all the edges of a graph are undirected, then the graph is called undirected. If $\mathcal{G}$ contains a sequence of edges of the form $(i_1,i_2),(i_2,i_3),\ldots,(i_k,i_{k+1})$, then the set $\{(i_1,i_2),(i_2,i_3),\ldots,(i_k,i_{k+1})\}$ is called a path of $\mathcal{G}$ from node i_1 to node i_{k+1} and node i_{k+1} is said to be reachable from node i_1. For an undirected graph, if there exists a path between any two different nodes, then it is called connected. A graph $\mathcal{G}$ is said to contain a spanning tree if there exists a node in $\mathcal{G}$ such that all the other nodes are reachable from it, and this node is called the root of the spanning tree. A matrix $\mathcal{A} = [a_{ij}] \in \mathbb{R}^{N\times N}$ is said to be a weighted adjacency matrix of a graph $\mathcal{G}$ if $a_{ii} = 0$; $a_{ij} > 0 \Leftrightarrow (j,i) \in \mathcal{E}$; and $a_{ij} = 0 \Leftrightarrow (j,i) \notin \mathcal{E}$. Moreover, for an undirected graph, $a_{ij} = a_{ji}$. Let $\mathcal{L} = [l_{ij}] \in \mathbb{R}^{N\times N}$ be such that $l_{ii} = \sum_{j=1}^{N} a_{ij}$ and $l_{ij} = -a_{ij}$ if $i \neq j$. $\mathcal{L}$ is called the Laplacian of $\mathcal{G}$ associated with the weighted adjacency matrix $\mathcal{A}$.

3 Problem formulation

Consider a FESMS with N heterogenous flywheel systems. For $i = 1\ldots,N$, as in Liu et al. (2021), the SOE dynamics of the ith flywheel are given by:

$$\dot{\phi}_i(t) = -\frac{2B_{vi}}{I_i}\phi_i(t) - \frac{2\gamma_i}{I_i}P_i(t) \tag{1}$$

where $\phi_i(t), I_i, B_{vi}$ denote the SOE, flywheel inertia, and friction coefficient, respectively. $\gamma_i = 1/\omega_{imax}^2$ with $\omega_{i\max}$ denoting the maximum admissible angular velocity of the ith flywheel. $P_i(t)$ is the net power output of the ith flywheel, where $P_i(t) > 0$ means power flow from flywheel to the grid, and $P_i(t) < 0$ vice versa. Here, $P_i(t)$ is taken as the control input.

Let

$$P_{FESMS}(t) = \sum_{i=1}^{N} P_i(t)$$

denote the power output of the entire FESMS, and $P_{REF}(t)$ denote the reference command for $P_{FESMS}(t)$, which is assumed to be generated by the following command generator

$$\dot{\eta}_0(t) = S_0\eta_0(t) \tag{2a}$$

$$P_{REF}(t) = C_0\eta_0(t) \tag{2b}$$

where $\eta_0(t) \in \mathbb{R}^q$ is the internal state of the command generator, $S_0 \in \mathbb{R}^{q\times q}$ and $C_0 \in \mathbb{R}^{1\times q}$ are constant matrices.

The communication network for the FESMS together with the command generator is modeled as a graph $\bar{\mathcal{G}} = (\bar{\mathcal{V}},\bar{\mathcal{E}})$, where $\bar{\mathcal{V}} = \{0,1,\ldots,N\}$ and $\bar{\mathcal{E}} \subseteq \{\bar{\mathcal{V}}\times\bar{\mathcal{V}}\}$. Here, the node 0 is associated with the command generator, and the node i is associated with the ith flywheel of the FESMS. For $i = 0,1,\ldots,N$, $j = 1,\ldots,N$, $(i,j) \in \bar{\mathcal{E}}$ if and only if the jth flywheel can receive the information from the command generator or the ith flywheel. Let $\mathcal{G} = (\mathcal{V},\mathcal{E})$ be a subgraph of $\bar{\mathcal{G}}$ with $\mathcal{V} = \{1,\ldots,N\}$ and $\mathcal{E} = \bar{\mathcal{E}} \cap \{\mathcal{V}\times\mathcal{V}\}$. Let $\bar{\mathcal{A}} = \left[a_{ij}\right] \in \mathbb{R}^{(N+1)\times(N+1)}$ be the weighted adjacency matrix of $\bar{\mathcal{G}}$ and $\mathcal{L}$ be the Laplacian of $\mathcal{G}$. The following assumption is imposed on the communication network.

Assumption 1. *The graph $\bar{\mathcal{G}}$ contains a spanning tree with node 0 as the root. Moreover, the graph $\mathcal{G}$ is undirected and connected.*

Assumption 1 means that the information of the command generator can be transmitted to each flywheel system through a communication path.

Now, the dual objective coordination problem for the FESMS is described as follows.

Problem 1. Given *systems (1), (2) and the communication network $\bar{\mathcal{G}}$, design a distributed control input P_i, such that*

$$\lim_{t\to\infty}\left(P_{FESMS}(t) - P_{REF}(t)\right) = 0, \tag{3}$$

and *for $i,j = 1,\ldots,N$, $i \neq j$,*

$$\lim_{t\to\infty}\left(\phi_i(t) - \phi_j(t)\right) = 0. \tag{4}$$

The control objective 3) means that the power output of the entire FESMS should meet its reference command, while the control objective 4) means that the SOE of all the flywheels should be balanced. To simultaneously achieve these two control objectives, the following lemma is established in Liu et al. (2021).

Lemma 1. *(Lemma 1 of* Liu et al. (2021)*) The following two equations simultaneously hold*

$$P_{FESMS}(t) = P_{REF}(t) \tag{5a}$$

$$\phi_i(t) = \phi_j(t),\ i,\quad j = 1,\ldots,N,\ i \neq j \tag{5b}$$

if and only if, for $i = 1,\ldots,N$, $\phi_i(t) = \psi_0(t)$, where $\psi_0(t)$ is governed by

$$\dot{\psi}_0(t) = -\alpha_0\psi_0(t) - \beta_0 P_{REF}(t) \tag{6}$$

with

$$\alpha_0 = \frac{2\sum_{i=1}^{N}\frac{B_{vi}}{\gamma_i}}{\sum_{j=1}^{N}\frac{I_i}{\gamma_i}},\ \beta_0 = \frac{2}{\sum_{i=1}^{N}\frac{I_i}{\gamma_i}}. \tag{7}$$

Lemma 1 reveals that the power tracking and SOE balancing control objectives together limit the SOE trajectories of all the

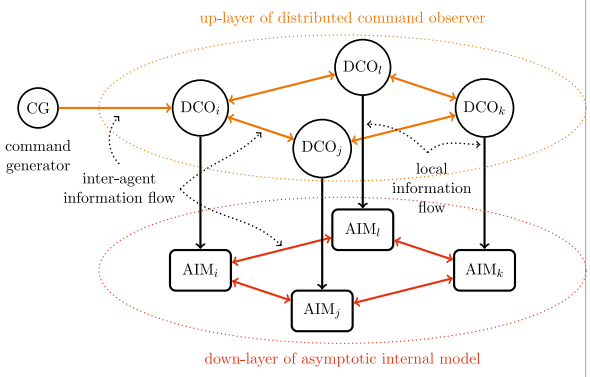

FIGURE 1
The inter-agent and local information flow regarding the two-layer control (8) and (9).

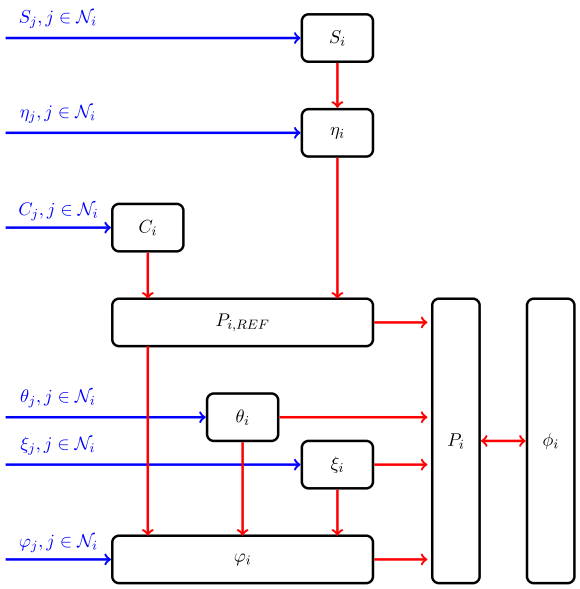

FIGURE 2
Information flow among the three parts of the control law (8)–(10).

flywheels to the solution of some common nonautonomous dynamic system (6), which is depicted by the system parameters of all the flywheels and takes the power reference command for the FESMS as the external input. Note that the system parameters B_{vi}, I_i and γ_i of all the flywheels are global system information. By directly taking system 6) as an external model, a distributed control approach was proposed in Liu et al. (2021) to solve Problem 1. However, the implementation of system 6) would not be possible without the acquirement of global system information and thus might not be feasible in practice. In this paper, an asymptotic internal model based method is further proposed to solve Problem 1, where, as will be proven later, system 6) turns out to be the common steady-state of all the asymptotic internal models of the flywheels. In this way, global system information is no longer required to solve Problem 1. The details of the asymptotic internal model based coordination will be given in the next section.

4 Asymptotic internal model based coordination

For $i = 1,\ldots,N$, the control law for the ith flywheel system consists of the following three parts:

1. Up-layer of distributed command observer

$$\dot{S}_i(t) = \mu_S \sum_{j=0}^{N} a_{ij}\left(S_j(t) - S_i(t)\right) \tag{8a}$$

$$\dot{C}_i(t) = \mu_C \sum_{j=0}^{N} a_{ij}\left(C_j(t) - C_i(t)\right) \tag{8b}$$

$$\dot{\eta}_i(t) = S_i(t)\,\eta_i(t) + \mu_\eta \sum_{j=0}^{N} a_{ij}\left(\eta_j(t) - \eta_i(t)\right) \tag{8c}$$

$$P_{i,REF}(t) = C_i(t)\,\eta_i(t) \tag{8}$$

2. Down-layer of asymptotic internal model

$$\dot{\theta}_i(t) = \mu_\theta \sum_{j=1}^{N} a_{ij}\left(\theta_j(t) - \theta_i(t)\right),\ \theta_i(0) = \frac{B_{vi}}{\gamma_i} \tag{9a}$$

$$\dot{\xi}_i(t) = \mu_\xi \sum_{j=1}^{N} a_{ij}\left(\xi_j(t) - \xi_i(t)\right),\ \xi_i(0) = \frac{I_i}{\gamma_i} \tag{9b}$$

$$\begin{aligned}\dot{\varphi}_i(t) = &-\frac{2\theta_i(t)}{\xi_i(t)}\varphi_i(t) - \frac{2}{N\xi_i(t)}P_{i,REF}(t)\\ &+ \mu_\varphi \sum_{j=1}^{N} a_{ij}\left(\varphi_j(t) - \varphi_i(t)\right),\ \varphi_i(0) = \phi_i(0)\end{aligned} \tag{9c}$$

3. Local SOE tracking controller

$$\begin{aligned}P_i(t) = -\frac{I_i}{2\gamma_i}\Bigg(&-\frac{2\theta_i(t)}{\xi_i(t)}\varphi_i(t) - \frac{2}{N\xi_i(t)}P_{i,REF}(t)\\ &- \kappa\left(\phi_i(t) - \varphi_i(t)\right) + \frac{2B_{vi}}{I_i}\phi_i(t)\Bigg)\end{aligned} \tag{10}$$

where $S_i(t) \in \mathbb{R}^{q\times q}$, $C_i(t) \in \mathbb{R}^{1\times q}$, $\eta_i(t) \in \mathbb{R}^q$, $P_{i,REF}(t) \in \mathbb{R}$ are the estimates of S_0, C_0, $\eta_0(t)$, and $P_{REF}(t)$, respectively. $\theta_i(t), \xi_i(t) \in \mathbb{R}$ are consensus parameters. $\varphi_i(t) \in \mathbb{R}$ is the state of the asymptotic internal model. $\mu_S, \mu_C, \mu_\eta, \mu_\theta, \mu_\xi, \mu_\varphi, \kappa$ are positive

TABLE 1 System friction, inertia and energy capacity parameters.

	B_{vi}	$I_i(\text{kg}\cdot\text{m}^2)$	$\omega_{i,\max}(\text{rad/s})$
Flywheel 1	1×10^{-3}	0.8	1,000
Flywheel 2	0.95×10^{-3}	0.9	800
Flywheel 3	1.05×10^{-3}	1.0	900
Flywheel 4	0.9×10^{-3}	1.3	1,200

control gains. The inter-agent and local information flow regarding the two-layer control 8) and 9) is illustrated by Figure 1, where "DCO" and "AIM" refer to distributed command observer and asymptotic internal model, respectively.

Now, we are ready to present the following main result.

Theorem 1. Given *systems (1), (2), under Assumption 1, if none of the eigenvalues of* S_0 *has positive real part, then the control law (8)-(10) solves Problem 1 for any* $\mu_S,\mu_C,\mu_\eta,\mu_\theta,\mu_\xi,\mu_\varphi,\kappa>0$.

Proof: For $i=1,\ldots,N$, let $\tilde{S}_i(t)=S_i(t)-S_0$, $\tilde{C}_i(t)=C_i(t)-C_0$, $\tilde{\eta}_i(t)=\eta_i(t)-\eta_0(t)$, $\tilde{P}_i(t)=P_{i,REF}(t)-P_{REF}(t)$. Then, by Theorem 4.6 of Cai et al. (2022), it follows that all $\tilde{S}_i(t)$, $\tilde{C}_i(t)$, $\tilde{\eta}_i(t)$ and $\tilde{P}_i(t)$ will all decay to zero exponentially.

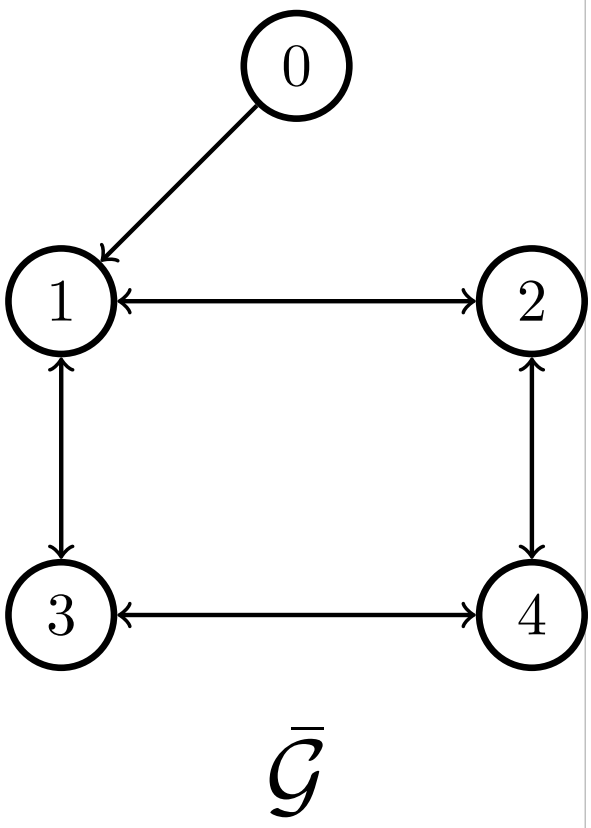

FIGURE 3
Communication network $\bar{\mathcal{G}}$.

Let $\theta(t)=\sum_{i=1}^N\theta_i(t)$. Since the graph $\mathcal{G}$ is undirected, $a_{ij}=a_{ji}$ for $i,j=1,\ldots,N$, $i\neq j$. Therefore,

$$\dot{\theta}(t)=\mu_\theta\sum_{i=1}^N\sum_{j=1}^N a_{ij}\left(\theta_j(t)-\theta_i(t)\right)=0 \tag{11}$$

which means for all $t\geq0$,

$$\theta(t)=\theta(0)=\sum_{i=1}^N\theta_i(0)=\sum_{i=1}^N\frac{B_{vi}}{\gamma_i}. \tag{12}$$

Moreover, by Corollary 2.9 of Ren and Beard (2008), under Assumption 1, all $\theta_i(t)$'s will reach consensus exponentially, i.e.,

$$\lim_{t\to\infty}\left(\theta_i(t)-\theta_j(t)\right)=0,\ i,\quad j=1,\ldots,N,\ i\neq j. \tag{13}$$

Therefore, for $i=1,\ldots,N$,

$$\lim_{t\to\infty}\theta_i(t)=\frac{\sum_{i=1}^N\frac{B_{vi}}{\gamma_i}}{N} \tag{14}$$

exponentially. Following the same procedure, for $i=1,\ldots,N$, it follows that

$$\lim_{t\to\infty}\xi_i(t)=\frac{\sum_{i=1}^N\frac{I_i}{\gamma_i}}{N} \tag{15}$$

exponentially. Since for all $i=1,\ldots,N$, $\theta_i(0)=\frac{B_{vi}}{\gamma_i}>0$, $\xi_i(0)=\frac{I_i}{\gamma_i}>0$, it follows that for all $t\geq0$, $\theta_i(t),\xi_i(t)>0$. As a result, control law (9c) and (10) are well imposed. Define

$$\alpha_i(t)=\frac{2\theta_i(t)}{\xi_i(t)}-\alpha_0,\ \beta_i(t)=\frac{2}{N\xi_i(t)}-\beta_0.$$

Then, by (7), 14 and 15, it follows that

$$\lim_{t\to\infty}\alpha_i(t)=0,\ \lim_{t\to\infty}\beta_i(t)=0 \tag{16}$$

exponentially.

Letting $\varphi(t)=\text{col}\ (\varphi_1(t),\ \ldots,\ \varphi_N(t))$, $\Delta_\alpha(t)=\text{diag}2\theta_1(t)/\xi_1(t),\ldots,2\theta_N(t)/\xi_N(t)$, and $\bar{P}(t)=\text{col}(2P_{1,REF}/N\xi_1(t),\ldots,2P_{N,REF}/N\xi_N(t))$ gives

$$\dot{\varphi}(t)=-\left(\Delta_\alpha(t)+\mu_\varphi\mathcal{L}\right)\varphi(t)-\bar{P}(t). \tag{17}$$

Note that $P_{REF}(t)$ must be bounded in practice, and thus $\bar{P}(t)$ will also be bounded. Since $\Delta_\alpha(t)+\mu_\varphi\mathcal{L}$ is positive definite for all $t\geq0$, $\varphi(t)$ will be bounded for all $t\geq0$.

Rewrite (9c) as follows

$$\begin{aligned}\dot{\varphi}_i(t)&=-\frac{2\theta_i(t)}{\xi_i(t)}\varphi_i(t)-\frac{2}{N\xi_i(t)}P_{i,REF}(t)\\&\quad+\mu_\varphi\sum_{j=1}^N a_{ij}\left(\varphi_j(t)-\varphi_i(t)\right)\\&=-\alpha_0\varphi_i(t)-\alpha_i(t)\varphi_i(t)-\beta_0P_{REF}(t)\\&\quad+\mu_\varphi\sum_{j=1}^N a_{ij}\left(\varphi_j(t)-\varphi_i(t)\right)\\&\quad+\beta_0P_{REF}(t)-\left(\beta_0+\beta_i(t)\right)\left(\tilde{P}_i(t)+P_{REF}(t)\right)\\&=-\alpha_0\varphi_i(t)-\beta_0P_{REF}(t)+\mu_\varphi\sum_{j=1}^N a_{ij}\left(\varphi_j(t)-\varphi_i(t)\right)\\&\quad+\delta_i(t)\end{aligned} \tag{18}$$

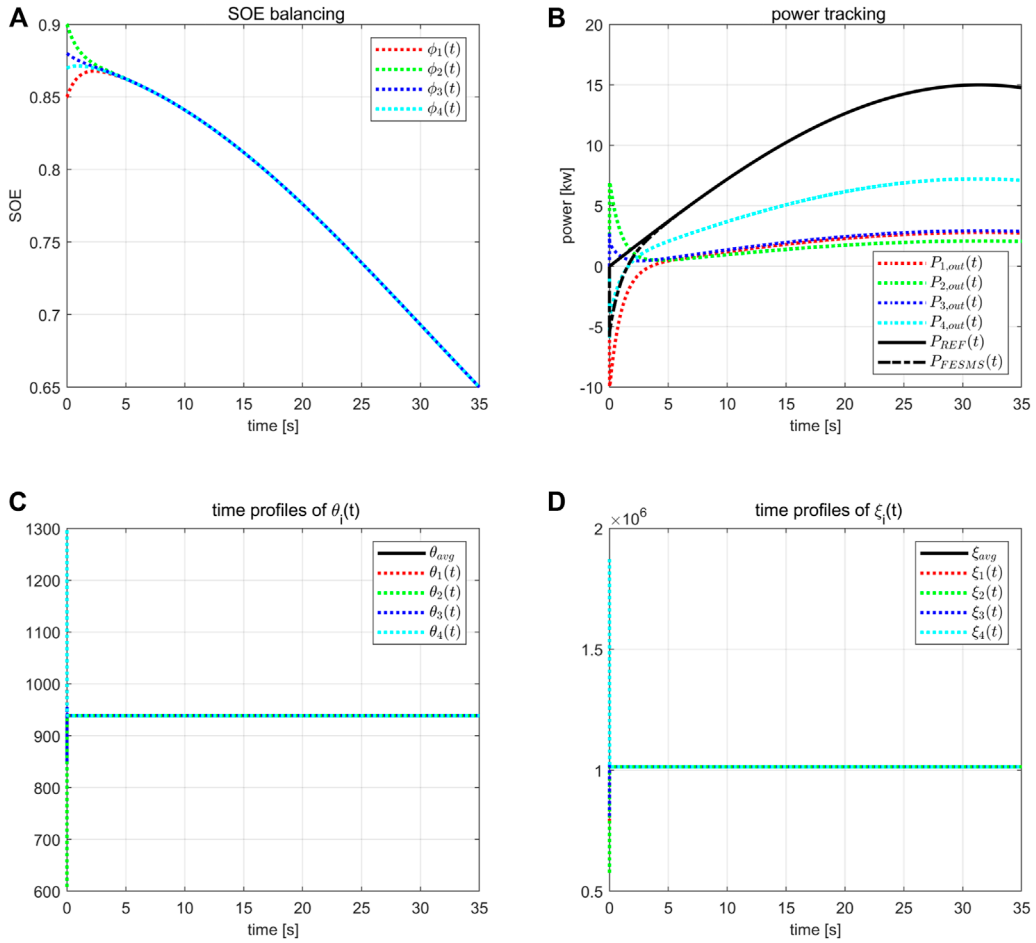

FIGURE 4
Control performance for the standard case.

where

$$\delta_i(t) = -\alpha_i(t)\varphi_i(t) + \beta_0 P_{REF}(t) - \left(\beta_0 + \beta_i(t)\right)\left(\tilde{P}_i(t) + P_{REF}(t)\right). \tag{19}$$

Since all $\alpha_i(t), \beta_i(t), \tilde{P}_i(t)$ tend to zero exponentially and $\varphi_i(t)$ is bounded, $\delta_i(t)$ also tends to zero exponentially. Let $\delta(t) = \mathrm{col}(\delta_1(t), \ldots, \delta_N(t))$. Then we have

$$\dot{\varphi}(t) = -\left(\alpha_0 I_N + \mu_\varphi \mathcal{L}\right)\varphi(t) - \beta_0 P_{REF}(t)\, 1_N + \delta(t). \tag{20}$$

Define $U = (U_1, U_r)$ where $U_1 = 1_N/\sqrt{N}$ and $U_r \in \mathbb{R}^{N\times(N-1)}$ is arbitrariliy chosen such that U is orthogonal. Then,

$$U^{-1} = U^T = \begin{pmatrix} U_1^T \\ U_r^T \end{pmatrix}. \tag{21}$$

Since $U^{-1}U = I_N$, $U_r^T U_1 = 0$. Therefore, $U^{-1}1_N = \mathrm{col}(\sqrt{N}, 0, \ldots, 0) \in \mathbb{R}^n$. Let $J = U_r^T \mathcal{L} U_r$. Since $\mathcal{L}1_N = 0$, we have $U^T \mathcal{L} U = \mathrm{block\ diag}\{0, J\}$. Then, under Assumption 1, J is symmetric and all the eigenvalues of J are positive. Let $\bar{\varphi}(t) = U^{-1}\varphi(t)$. Then we have

$$\begin{aligned} \dot{\bar{\varphi}}(t) &= -U^{-1}\left(\alpha_0 I_N + \mu_\varphi \mathcal{L}\right)\varphi(t) \\ &\quad - \beta_0 P_{REF}(t)\, U^{-1} 1_N + U^{-1}\delta(t) \\ &= -U^{-1}\left(\alpha_0 I_N + \mu_\varphi \mathcal{L}\right) U\bar{\varphi}(t) \\ &\quad - \beta_0 P_{REF}(t)\, U^{-1} 1_N + U^{-1}\delta(t) \\ &= -\left(\alpha_0 I_N + \mu_\varphi U^{-1}\mathcal{L}U\right)\bar{\varphi}(t) \\ &\quad - \beta_0 P_{REF}(t)\, U^{-1} 1_N + \bar{\delta}(t) \end{aligned} \tag{22}$$

where $\bar{\delta}(t) = U^{-1}\delta(t)$. Let $\bar{\varphi}(t) = \mathrm{col}(\bar{\varphi}_s(t), \bar{\varphi}_t(t))$, $\bar{\delta}(t) = \mathrm{col}(\bar{\delta}_s(t), \bar{\delta}_t(t))$ with $\bar{\varphi}_s(t), \bar{\delta}_s(t) \in \mathbb{R}$ and $\bar{\varphi}_t(t), \bar{\delta}_t(t) \in \mathbb{R}^{N-1}$. Then system (22) can be split into the following two subsystems

$$\dot{\bar{\varphi}}_s(t) = -\alpha_0 \bar{\varphi}_s(t) - \beta_0 \sqrt{N} P_{REF}(t) + \bar{\delta}_s(t) \tag{23a}$$

$$\dot{\bar{\varphi}}_t(t) = -\left(\alpha_0 I_{N-1} + \mu_\varphi J\right)\bar{\varphi}_t(t) + \bar{\delta}_t(t). \tag{23b}$$

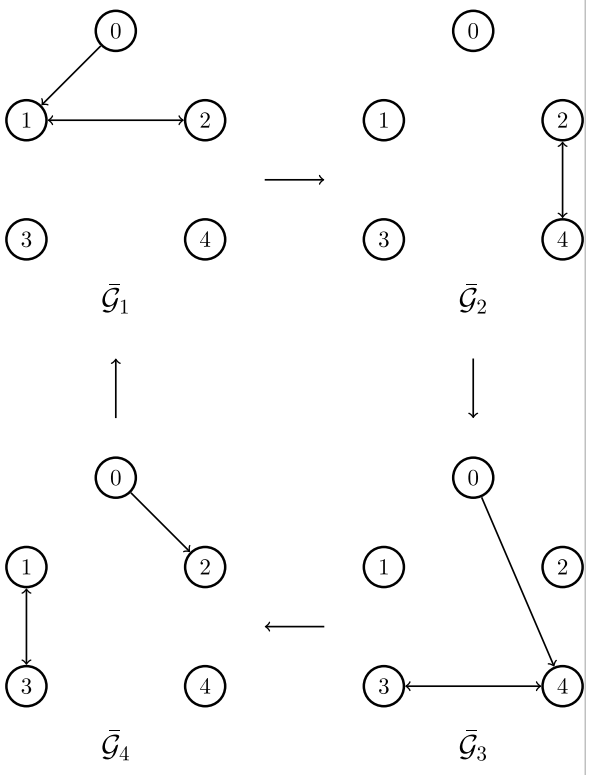

FIGURE 5
Unreliable switched communication network $\bar{\mathcal{G}}$.

Since $\bar{\delta}_t(t)$ tends to zero exponentially and $\alpha_0 I_{N-1} + \mu_\varphi J$ is positive definite, it follows that $\bar{\varphi}_t(t)$ tends to zero exponetially. As a result, by noting that

$$\varphi(t) = U\bar{\varphi}(t) = (U_1, U_r)\begin{pmatrix}\bar{\varphi}_s(t)\\ \bar{\varphi}_t(t)\end{pmatrix} = U_1\bar{\varphi}_s(t) + U_r\bar{\varphi}_t(t) \tag{24}$$

it concludes that

$$\lim_{t\to\infty}\left(\varphi(t) - \left(\bar{\varphi}_s(t)/\sqrt{N}\right)1_N\right) = 0 \tag{25}$$

i.e.,

$$\lim_{t\to\infty}\left(\varphi_i(t) - \varphi_j(t)\right) = 0,\ i,\quad j = 1,\ldots,N,\ i \neq j. \tag{26}$$

Furthermore, by 9c and 16, it follows that there implicitly exists a nonautonomous dynamic system (6) such that $\lim_{t\to\infty}(\varphi_i(t) - \psi_0(t)) = 0$ for all $i = 1,\ldots,N$. Then, by Lemma 1, it suffices to show $\lim_{t\to\infty}(\phi_i(t) - \varphi_i(t)) = 0$.

Submitting (10) into 1) gives

$$\begin{aligned}\dot{\phi}_i(t) &= -\frac{2B_{vi}}{I_i}\phi_i(t) + \frac{2\gamma_i}{I_i}\frac{I_i}{2\gamma_i}\left(-\frac{2\theta_i(t)}{\xi_i(t)}\varphi_i(t) - \frac{2}{N\xi_i(t)}\right.\\ &\quad\left.\times P_{i,REF}(t) - \kappa(\phi_i(t) - \varphi_i(t)) + \frac{2B_{vi}}{I_i}\phi_i(t)\right)\\ &= -\frac{2\theta_i(t)}{\xi_i(t)}\varphi_i(t) - \frac{2}{N\xi_i(t)}P_{i,REF}(t) - \kappa(\phi_i(t) - \varphi_i(t)).\end{aligned} \tag{27}$$

Define $\bar{\phi}_i(t) = \phi_i(t) - \varphi_i(t)$. Then we have

$$\begin{aligned}\dot{\bar{\phi}}_i(t) &= -\frac{2\theta_i(t)}{\xi_i(t)}\varphi_i(t) - \frac{2}{N\xi_i(t)}P_{i,REF}(t) - \kappa(\phi_i(t) - \varphi_i(t))\\ &\quad + \frac{2\theta_i(t)}{\xi_i(t)}\varphi_i(t) + \frac{2}{N\xi_i(t)}P_{i,REF}(t)\\ &\quad - \mu_\varphi\sum_{j=1}^{N}a_{ij}\left(\varphi_j(t) - \varphi_i(t)\right)\\ &= -\kappa\bar{\phi}_i(t) - \mu_\varphi\sum_{j=1}^{N}a_{ij}\left(\varphi_j(t) - \varphi_i(t)\right).\end{aligned} \tag{28}$$

Since $\kappa > 0$, by (26), it follows that $\lim_{t\to\infty}\bar{\phi}_i(t) = 0$ and the proof is thus complete.

The working principle for the asymptotic internal model 9) is as follows. First, the consensus algorithms (9a) and (9b) are adopted to estimate the global system information α_0 and β_0. Based on the esitmated α_0 and β_0, i.e., $2\theta_i(t)/\xi_i(t)$ and $2/N\xi_i(t)$, a local certainty equivalent internal model is ready. Then, more importantly, the states of the internal models of all the flywheels should reach a common trajectory. To this end, the consensus term $\mu_\varphi\sum_{j=1}^{N}a_{ij}(\varphi_j(t) - \varphi_i(t))$ is resorted to and added to the dynamics of the internal mode, which makes it an asymptotic internal mode in the sense that the states of all the internal models will eventually reach a common trajectory.

The information flow among the three parts of the control law (8)–(10) is shown in Figure 2.

5 Case studies

In this section, we consider a FESMS consisting of four flywheels as in Liu et al. (2021). The system parameters are given in Table 1, which come from the works in Ghanaatian and Lotfifard (2019); Liu et al. (2021). Moreover, the communication graph $\bar{\mathcal{G}}$ is shown in Figure 3, where node 0 represents the command generator, and node i represents the ith flywheel, $i = 1,\ldots,4$. The command generator is designed as

$$\begin{aligned}\dot{\eta}_0(t) &= \begin{pmatrix}0 & 0.05\\ -0.05 & 0\end{pmatrix}\eta_0(t)\\ \eta_0(0) &= \begin{pmatrix}0\\ 2.5\times10^4\end{pmatrix}\\ P_{REF}(t) &= \begin{pmatrix}1 & 0\end{pmatrix}\eta_0(t).\end{aligned} \tag{29}$$

Thus, $P_{REF}(t) = 25\sin(0.05t)$ kw. In what follows, we will conduct case studies in different scenarios to examine the performance of the proposed control method.

Case 1: standard case.

The control gains are selected to be

$$\mu_S = \mu_C = \mu_\eta = \mu_\theta = \mu_\xi = \mu_\varphi = 100$$

and $\kappa = 1$. The system initial values are given by

$$\phi_1(0) = \varphi_1(0) = 0.85,\ \phi_2(0) = \varphi_2(0) = 0.9$$
$$\phi_3(0) = \varphi_3(0) = 0.88,\ \phi_4(0) = \varphi_4(0) = 0.87$$

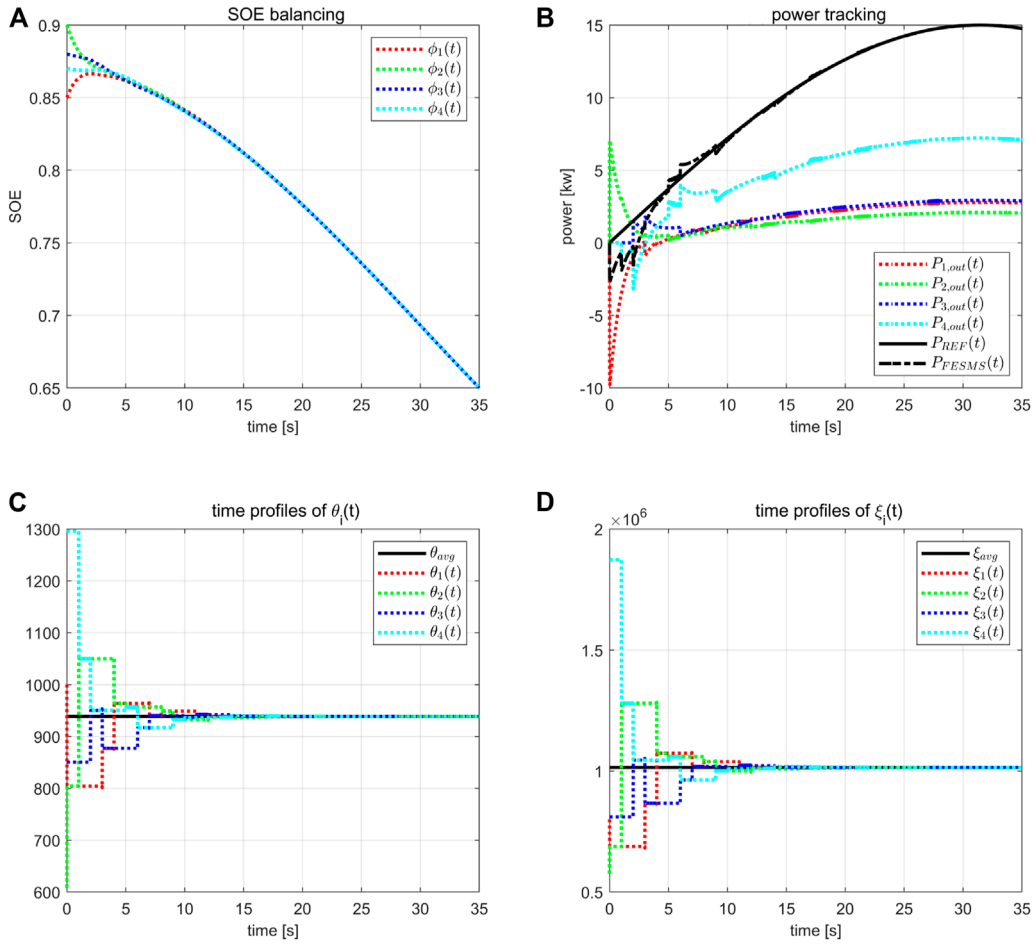

FIGURE 6
Control performance subject to unreliable communication links.

and for $i = 1, 2, 3, 4$,

$$S_i(0) = 0,\ C_i(0) = 0,\ \eta_i(0) = 0.$$

The system performance is shown by Figure 4. It can be seen from subfigures (a) and (b) that both SOE balancing and power tracking have been successfully achieved. Moreover, let

$$\theta_{avg} = \frac{\sum_{i=1}^{N} \frac{B_{vi}}{\gamma_i}}{N},\ \xi_{avg} = \frac{\sum_{i=1}^{N} \frac{I_i}{\gamma_i}}{N}.$$

Then by subfigures (c) and (d), it can be observed that $\theta_i(t)$ and $\xi_i(t)$ converge to θ_{avg} and ξ_{avg}, respectively. Thus, the external model as in Liu et al. (2021) is no longer required, which depends on the global system information of θ_{avg} and ξ_{avg}.

Case 2: effect of unreliable communication links.

In the standard case, we assume the communication network to be static and reliable. While, in practice, due to malicious attack or equipment failure, the communication links might not always be reliable. In this case, we will check the control performance of the proposed control method subject to unreliable communication links. In particular, the communication network is assumed to switch among four subgraphs $\bar{\mathcal{G}}_1$, $\bar{\mathcal{G}}_2$, $\bar{\mathcal{G}}_3$, $\bar{\mathcal{G}}_4$ periodically every 1s, as shown in Figure 5. The same control gains and system initial values as in Case 1 are employed. The system performance is shown by Figure 6. By subfigures (a) and (b), it can be seen the proposed control method shows certain robustness against unreliable communication links in the sense that the control objectives of SOE balancing and power tracking can still be achieved, though requiring longer time to reach steady state. Moreover, once the steady state is reached, the effect of the unreliable communication links would be minor. Similarly, it also takes longer time for $\theta_i(t)$ and $\xi_i(t)$ to reach consensus. Note that for all the four subgraphs $\bar{\mathcal{G}}_1$, $\bar{\mathcal{G}}_2$, $\bar{\mathcal{G}}_3$, $\bar{\mathcal{G}}_4$, the communication links between flywheels are undirected. If these links become directed, then the average consensus on $\theta_i(t)$ and $\xi_i(t)$ might be violated.

Case 3: effect of power output saturation.

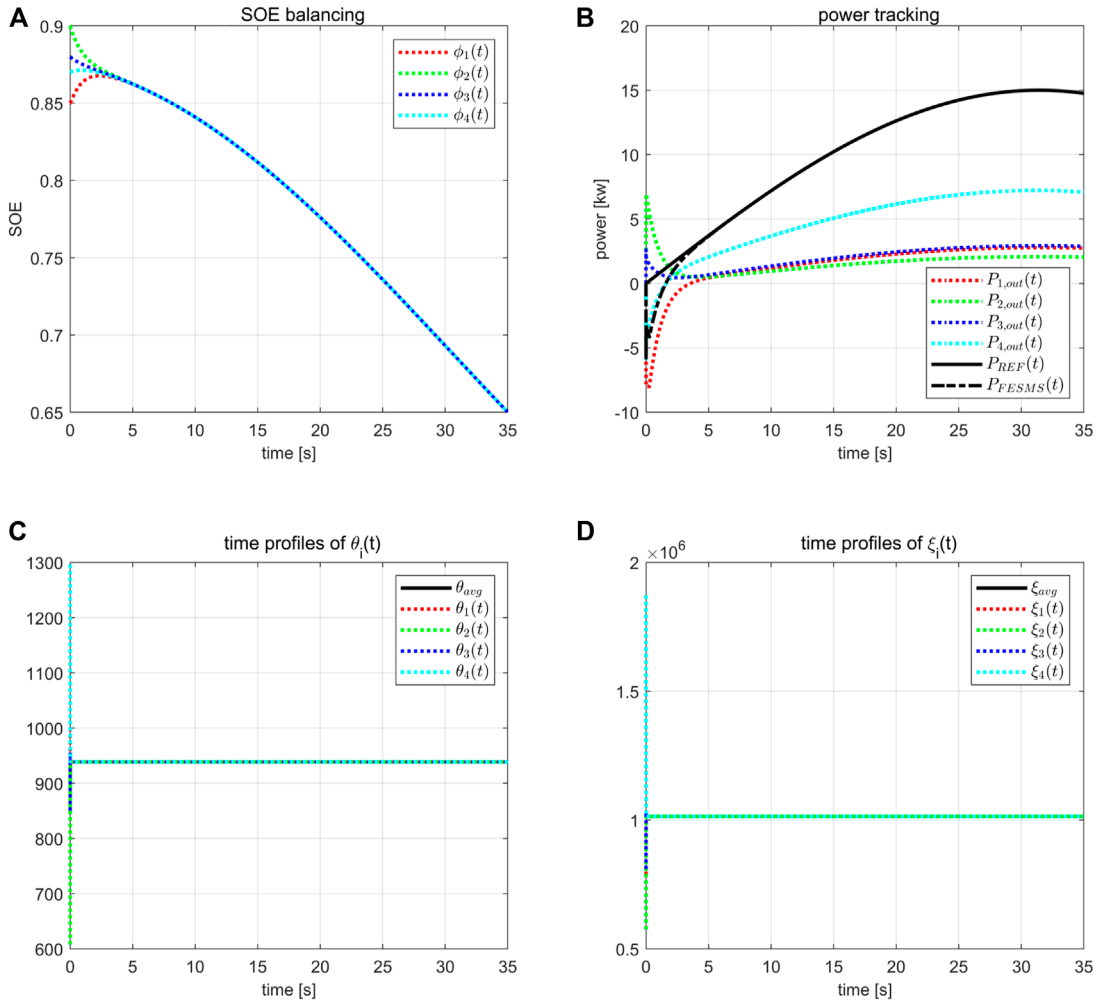

FIGURE 7
Control performance subject to power output saturation.

In practice, the power output of the flywheel is always subject to saturation. In this case, we will consider the effect of power output saturation. Suppose

$$P_i(t) = \begin{cases} P_\alpha, & P_i(t) \geq P_\alpha; \\ P_\beta, & P_i(t) \leq P_\beta; \\ P_i(t), & \text{otherwise.} \end{cases}$$

where $P_\alpha > 0$ and $P_\beta < 0$ are the limits. In the simulation, we let $P_\alpha = -P_\beta = 8$kw. The same control gains and system initial values as in Case 1 are employed. The system performance is shown by Figure 7. It can be seen that as long as the saturation does not conflict with the steady-state power output, both the control objectives of SOE balancing and power tracking can still be achieved, which means that the saturation function can be directly applied to the proposed power control input.

Case 4: effect of time-delay.

In this case, we check the effect of time-delay of the communication network on the control performance. Consider a constant inter-system time-delay, where the time-delay between flywheel 1 and flywheel two is 1×10^{-4}sec; between flywheel two and flywheel four is 2×10^{-4}sec; between flywheel three and flywheel four is 3×10^{-4}sec; between flywheel 1 and flywheel three is 4×10^{-4}sec. The same control gains and system initial values as in Case 1 are employed. The system performance is shown by Figure 8. It can be seen that though the SOE balancing control objective can be achieved, the power tracking cannot be exactly realized. In this sense, the proposed control method shows certain sensitivity to time-delay. In general, the longer the time-delay is, the worse the control performance is. It would be an interesting topic to consider how to compensate the communication time-delay in the future. Nevertheless,

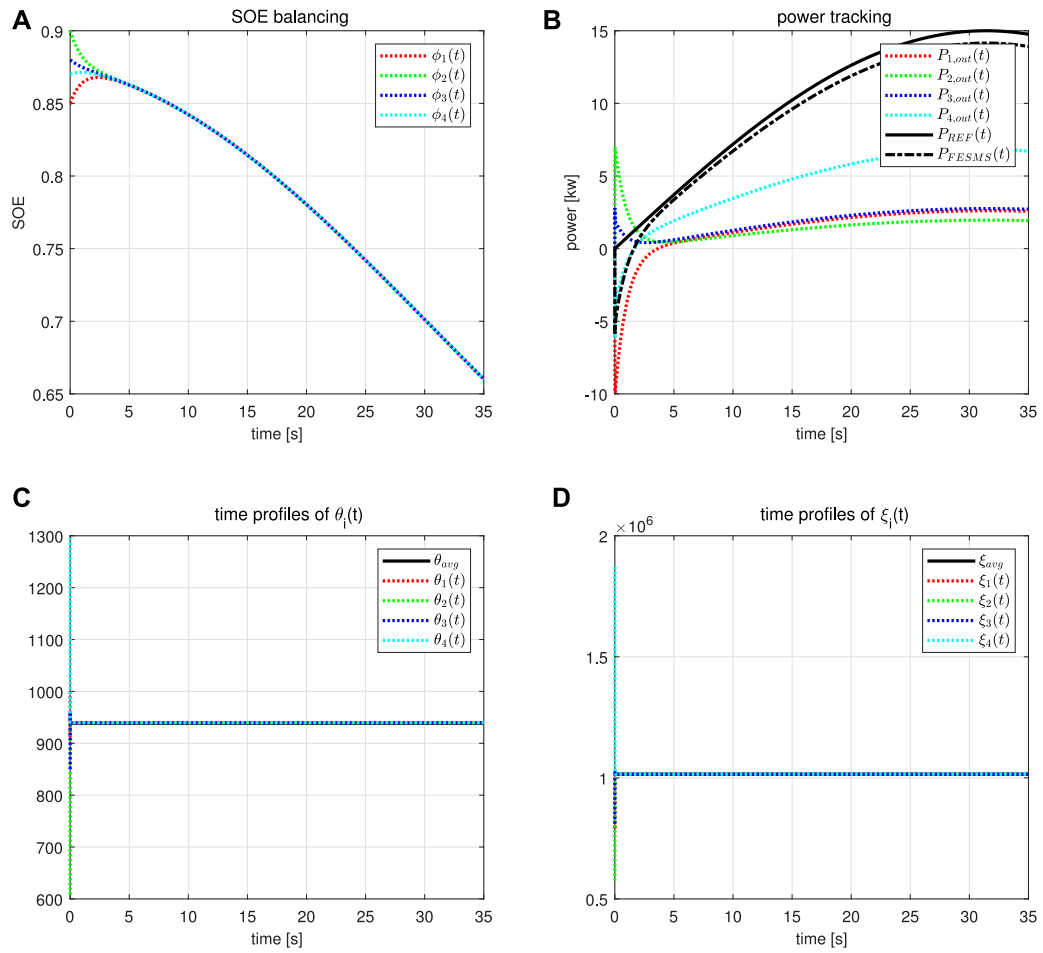

FIGURE 8
Control performance subject to time-delay.

in practice, the time-delay over normal transmission lines is usually on the order of 5×10^{-7}sec/100m. Therefore, the proposed control method will be definitely feasible for cable communication network.

6 Conclusion

This paper considers the dual objective distributed coordination problem for a FESMS. To eliminate the need of an external model which depends on global system information as in Liu et al. (2021), a novel asymptotic internal model based control method is proposed in this paper by taking advantage of the average consensus algorithms. It is proven that the steady-state of the asymptotic internal model turns out to be a common state-of-energy generator for all the flywheels, which lends itself to the solution to the dual objective distributed coordination problem.

Comprehensive numerical case studies show that the proposed control method has certain robustness against unreliable communication links and time-delay in information transmission. While, the unreliable communication would result in undesired oscillations in system transient response, and the information transmission delay would lead to steady-state tracking errors regarding power dispatch. Moreover, we also consider the constraint on power output saturation for the flywheels, and the obtained results indicate that the proposed control method can be directly integrated with the power limits without destabilizing the closed-loop system.

It is worth mentioning that in this paper, only homogeneous flywheel energy storage units are considered which are governed by the dynamic **Eq. 1**. Nevertheless, the proposed control approach can also handle the dual objective control problem for an energy storage system made up of heterogeneous energy storage units whose dynamic equations are in the same form of **Eq. 1**. While, it would be interesting to consider the

dual objective control problem for an energy storage system with heterogeneous energy storage units of different dynamic equations in the future.

Data availability statement

The original contributions presented in the study are included in the article/Supplementary material, further inquiries can be directed to the corresponding author.

Author contributions

HC contributed to all the contents of this paper.

Funding

This work was supported in part by the National Nature Science Foundation of China under Grant 61803160, and in part by the Guangdong Nature Science Foundation under Grant 2020A1515010810.

Conflict of interest

The author declares that the research was conducted in the absence of any commercial or financial relationships that could be construed as a potential conflict of interest.

Publisher's note

References

Ahamad, N. B. b., Su, C.-L., Zhaoxia, X., Vasquez, J. C., Guerrero, J. M., and Liao, C.-H. (2019). Energy harvesting from harbor cranes with flywheel energy storage systems. *IEEE Trans. Ind. Appl.* 55, 3354–3364. doi:10.1109/TIA.2019.2910495

Akram, U., Nadarajah, M., Shah, R., and Milano, F. (2020). A review on rapid responsive energy storage technologies for frequency regulation in modern power systems. *Renew. Sustain. Energy Rev.* 120, 109626. doi:10.1016/j.rser.2019.109626

Amiryar, M. E., and Pullen, K. R. (2017). A review of flywheel energy storage system technologies and their applications. *Appl. Sci.* 7, 286. doi:10.3390/app7030286

Arani, A. K., Karami, H., Gharehpetian, G., and Hejazi, M. (2017). Review of flywheel energy storage systems structures and applications in power systems and microgrids. *Renew. Sustain. Energy Rev.* 69, 9–18. doi:10.1016/j.rser.2016.11.166

Cai, H., and Hu, G. (2016). Distributed control scheme for package-level state-of-charge balancing of grid-connected battery energy storage system. *IEEE Trans. Ind. Inf.* 12, 1919–1929. doi:10.1109/TII.2016.2601904

Cai, H., Su, Y., and Huang, J. (2022). *Cooperative control of multi-agent systems: Distributed-observer and distributed-internal-model approaches*. Switzerland: Springer Cham.

Canova, A., Campanelli, F., and Quercio, M. (2022). Flywheel energy storage system in Italian regional transport railways: A case study. *Energies* 15, 1096. doi:10.3390/en15031096

Cao, Q., Song, Y.-D., Guerrero, J. M., and Tian, S. (2016). Coordinated control for flywheel energy storage matrix systems for wind farm based on charging/discharging ratio consensus algorithms. *IEEE Trans. Smart Grid* 7, 1259–1267. doi:10.1109/TSG.2015.2470543

Chang, X., Li, Y., Zhang, W., Wang, N., and Xue, W. (2015). Active disturbance rejection control for a flywheel energy storage system. *IEEE Trans. Ind. Electron.* 62, 991–1001. doi:10.1109/TIE.2014.2336607

Choudhury, S. (2021). Flywheel energy storage systems: A critical review on technologies, applications, and future prospects. *Int. Trans. Electr. Energy Syst.* 31, e13024. doi:10.1002/2050-7038.13024

Daoud, M. I., Massoud, A. M., Abdel-Khalik, A. S., Elserougi, A., and Ahmed, S. (2016). A flywheel energy storage system for fault ride through support of grid-connected vsc hvdc-based offshore wind farms. *IEEE Trans. Power Syst.* 31, 1671–1680. doi:10.1109/TPWRS.2015.2465163

Faisal, M., Hannan, M. A., Ker, P. J., Hussain, A., Mansor, M. B., and Blaabjerg, F. (2018). Review of energy storage system technologies in microgrid applications: Issues and challenges. *IEEE Access* 6, 35143–35164. doi:10.1109/ACCESS.2018.2841407

Gengji, W., and Ping, W. (2016). Rotor loss analysis of pmsm in flywheel energy storage system as uninterruptable power supply. *IEEE Trans. Appl. Supercond.* 26, 1–5. doi:10.1109/TASC.2016.2594826

Ghanaatian, M., and Lotfifard, S. (2019). Control of flywheel energy storage systems in the presence of uncertainties. *IEEE Trans. Sustain. Energy* 10, 36–45. doi:10.1109/TSTE.2018.2822281

Gong, L., Wang, M., and Zhu, C. (2020). Immersion and invariance manifold adaptive control of the dc-link voltage in flywheel energy storage system discharge. *IEEE Access* 8, 144489–144502. doi:10.1109/ACCESS.2020.3013137

He, H., Liu, Y., and Ba, L. (2022). A nonlinear dynamic model of flywheel energy storage systems based on alternative concept of back propagation neural networks. *J. Comput. Nonlinear Dyn.* 17. doi:10.1115/1.4054681

Jia, Y., Wu, Z., Zhang, J., Yang, P., and Zhang, Z. (2022). Control strategy of flywheel energy storage system based on primary frequency modulation of wind power. *Energies* 15, 1850. doi:10.3390/en15051850

Lai, J., Song, Y., and Du, X. (2018). Hierarchical coordinated control of flywheel energy storage matrix systems for wind farms. *Ieee. ASME. Trans. Mechatron.* 23, 48–56. doi:10.1109/TMECH.2017.2654067

Li, J., Xin, D., Wang, H., and Liu, C. (2022a). "Application of energy storage system in rail transit: A review," in In 2022 International Conference on Power Energy Systems and Applications, Singapore, Singapore, 25-27 February 2022 (Singapore: ICoPESA), 539–552. doi:10.1109/ICoPESA54515.2022.9754481

Li, X., Anvari, B., Palazzolo, A., Wang, Z., and Toliyat, H. (2018). A utility-scale flywheel energy storage system with a shaftless, hubless, high-strength steel rotor. *IEEE Trans. Ind. Electron.* 65, 6667–6675. doi:10.1109/TIE.2017.2772205

Li, X., and Palazzolo, A. (2022). A review of flywheel energy storage systems: State of the art and opportunities. *J. Energy Storage* 46, 103576. doi:10.1016/j.est.2021.103576

Li, Z., Nie, Z., Xu, J., Li, H., and Ai, S. (2022b). Harmonic analysis and neutral-point potential control of interleaved parallel three-level inverters for flywheel energy storage system. *Front. Energy Res.* 9, 811845. doi:10.3389/fenrg.2021.811845

Liang, Y., Liang, D., Kou, P., Jia, S., Chu, S., Wang, H., et al. (2022). Linear robust discharge control for flywheel energy storage system with rlc filter. *IEEE Trans. Industry Appl.* 1, 15. doi:10.1109/TIA.2022.3189967

Liu, H., Gao, H., Guo, S., and Cai, H. (2021). Coordination of a flywheel energy storage matrix system: An external model approach. *IEEE Access* 9, 34475–34486. doi:10.1109/ACCESS.2021.3061743

Lu, X., Sun, K., Guerrero, J. M., Vasquez, J. C., and Huang, L. (2015). Double-quadrant state-of-charge-based droop control method for distributed energy storage systems in autonomous dc microgrids. *IEEE Trans. Smart Grid* 6, 147–157. doi:10.1109/TSG.2014.2352342

Lu, X., Sun, K., Guerrero, J. M., Vasquez, J. C., and Huang, L. (2014). State-of-charge balance using adaptive droop control for distributed energy storage systems in dc microgrid applications. *IEEE Trans. Ind. Electron.* 61, 2804–2815. doi:10.1109/TIE.2013.2279374

Morstyn, T., Hredzak, B., and Agelidis, V. G. (2016). Cooperative multi-agent control of heterogeneous storage devices distributed in a dc microgrid. *IEEE Trans. Power Syst.* 31, 2974–2986. doi:10.1109/TPWRS.2015.2469725

Morstyn, T., Savkin, A. V., Hredzak, B., and Agelidis, V. G. (2018). Multi-agent sliding mode control for state of charge balancing between battery energy storage systems distributed in a dc microgrid. *IEEE Trans. Smart Grid* 9, 4735–4743. doi:10.1109/TSG.2017.2668767

Mousavi, G. S., Faraji, F., Majazi, A., and Al-Haddad, K. (2017). A comprehensive review of flywheel energy storage system technology. *Renew. Sustain. Energy Rev.* 67, 477–490. doi:10.1016/j.rser.2016.09.060

Olabi, A. G., Wilberforce, T., Abdelkareem, M. A., and Ramadan, M. (2021). Critical review of flywheel energy storage system. *Energies* 14, 2159. doi:10.3390/en14082159

Ren, W., and Beard, R. W. (2008). *Distributed consensus in multi-vehicle cooperative control:theory and applications*. London: Springer.

Shi, C., Wei, T., Tang, X., Zhou, L., and Zhang, T. (2019). Charging–discharging control strategy for a flywheel array energy storage system based on the equal incremental principle. *Energies* 12, 2844. doi:10.3390/en12152844

Sun, Y., Hu, J., and Liu, J. (2020). Periodic event-triggered control of flywheel energy storage matrix systems for wind farms. *IET Control Theory &amp. Appl.* 14, 1467–1477. doi:10.1049/iet-cta.2018.5731

Thormann, B., Puchbauer, P., and Kienberger, T. (2021). Analyzing the suitability of flywheel energy storage systems for supplying high-power charging e-mobility use cases. *J. Energy Storage* 39, 102615. doi:10.1016/j.est.2021.102615

Tomczewski, A., Kasprzyk, L., and Nadolny, Z. (2019). Reduction of power production costs in a wind power plant–flywheel energy storage system arrangement. *Energies* 12, 1942. doi:10.3390/en12101942

Wei, G., Jiancheng, Z., Chong, L., and Hao, S. (2018). Control method of flywheel energy storage array for grid-connected wind-storage microgrid. *Energy Storage Sci. Technol.* 7, 810. doi:10.12028/j.issn.2095-4239.2018.0013

Yin, L., and Li, Y. (2022). Fuzzy vector reinforcement learning algorithm for generation control of power systems considering flywheel energy storage. *Appl. Soft Comput.* 125, 109149. doi:10.1016/j.asoc.2022.109149

Zhang, W., Li, Y., Wu, G., Rao, Z., Gao, J., and Luo, D. (2021). Robust predictive power control of n*3-phase pmsm for flywheel energy storage systems application. *Energies* 14, 3684. doi:10.3390/en14123684

Zhang, X., and Yang, J. (2018). A dc-link voltage fast control strategy for high-speed pmsm/g in flywheel energy storage system. *IEEE Trans. Ind. Appl.* 54, 1671–1679. doi:10.1109/TIA.2017.2783330

Zhang, X., and Yang, J. (2017). A robust flywheel energy storage system discharge strategy for wide speed range operation. *IEEE Trans. Ind. Electron.* 64, 7862–7873. doi:10.1109/TIE.2017.2694348

Zhang, Z., Meng, K., Liu, Q., and Wu, H. (2022). Hierarchical energy coordination of flywheel energy storage array system for wind farms based on consensus algorithm. *AIP Adv.* 12, 035005. doi:10.1063/5.0083391

Nomenclature

$\boldsymbol{\phi_i(t)}$ The SOE of the *i*th flywheel

$\boldsymbol{P_i(t)}$ the net power output of the *i*th flywheel

$\boldsymbol{B_{vi}}$ the friction coefficient of the *i*th flywheel

$\boldsymbol{I_i}$ the inertia of the *i*th flywheel

$\boldsymbol{\omega_{imax}}$ the maximum admissible angular velocity of the *i*th flywheel

$\boldsymbol{\gamma_i}$ $1/\omega_{\text{imax}}{}^2$

$\boldsymbol{P_{FESMS}(t)}$ the power output of the entire FESMS

$\boldsymbol{P_{REF}(t)}$ the reference command for $P_{FESMS}(t)$

$\boldsymbol{S_0}$ the system matrix of the command generator

$\boldsymbol{C_0}$ the output matrix of the command generator

$\boldsymbol{\eta_0(t)}$ the internal state of the command generator

$\bar{\mathcal{G}}$ the communication graph

$\boldsymbol{\phi_0(t)}$ the common trajectory for all the flywheels

$\boldsymbol{\alpha_0, \beta_0}$ the system parameters governing the common trajectory

$\boldsymbol{S_i(t)}$ the estimation of matrix S_0 by the *i*th flywheel

$\boldsymbol{C_i(t)}$ the estimation of matrix C_0 by the *i*th flywheel

$\boldsymbol{\eta_i(t)}$ the estimation of η_0 by the *i*th flywheel

$\boldsymbol{P_{i,REF}(t)}$ the estimation of $P_{REF}(t)$ by the *i*th flywheel

$\boldsymbol{\theta_i(t)}$ the consensus parameter for B_{vi}/γ_i of the *i*th flywheel

$\boldsymbol{\xi_i(t)}$ the consensus parameter for I_i/γ_i of the *i*th flywheel

$\boldsymbol{\varphi_i(t)}$ the state of the asymptotic internal model of the *i*th flywheel

$\boldsymbol{\alpha_i(t), \beta_i(t)}$ the estimation of α_0 and β_0 by the *i*th flywheel, respectively